



The structural basis of the low catalytic activities of the two minor β -carbonic anhydrases of the filamentous fungus *Aspergillus fumigatus*

Songwon Kim, Na Jin Kim, Semi Hong, Subin Kim, Jongmin Sung, Mi Sun Jin*

School of Life Sciences, GIST, 123 Cheomdan-gwagiro, Buk-gu, Gwangju 61005, Republic of Korea

ARTICLE INFO

Keywords:
 β -class carbonic anhydrase
Aspergillus fumigatus
 CafC
 CafD
 Low catalytic activity

ABSTRACT

The β -carbonic anhydrases (β -CAs) are widely distributed zinc-metalloenzymes that play essential roles in growth, survival, development and virulence in fungi. The majority of filamentous ascomycetes possess multiple β -CA isoforms among which major and minor forms have been characterized. We examined the catalytic behavior of the two minor β -CAs, CafC and CafD, of *Aspergillus fumigatus*, and found that both enzymes exhibited low CO₂ hydration activities. To understand the structural basis of their low activities, we performed X-ray crystallographic and site-directed mutagenesis studies. Both enzymes exist as homodimers. Like other Type-I β -CAs, the CafC active site has an “open” conformation in which the zinc ion is tetrahedrally coordinated by three residues (C36, H88 and C91) and a water molecule. However, L25 and L78 on the rim of the catalytic entry site protrude into the active site cleft, partially occluding access to it. Single (L25G or L78G) and double mutants provided evidence that widening the entrance to the active site greatly accelerates catalytic activity. By contrast, CafD has a typical Type-II “closed” conformation in which the zinc-bound water molecule is replaced by aspartic acid (D36). The most likely explanation for this result is that an arginine that is largely conserved within the β -CA family is replaced by glycine (G38), so that D36 cannot undergo a conformational change by forming a D-R pair that creates the space for a zinc-bound water molecule and switches the enzyme to the active form. The CafD structure also reveals the presence of a “non-catalytic” zinc ion in the dimer interface, which may contribute to stabilizing the dimeric assembly.

1. Introduction

Carbon dioxide (CO₂) is a key molecule in many physiological processes. It is produced as a waste product of cellular respiration and serves as raw material for photosynthesis in plants (Badger and Price, 1994). In nature, CO₂ exists in equilibrium with bicarbonate (HCO₃[−]) and protons. The interconversion of CO₂ and bicarbonate is slow, but can be accelerated by the zinc-metalloenzyme carbonic anhydrases (CAs), with k_{cat} values up to $\sim 10^6$ per second (Hasinoff, 1984; Pocker and Janjić, 1987). CAs are currently classified into seven families (α , β , γ , δ , ζ , η and θ) (Del Prete et al., 2014a; Del Prete et al., 2014b; Iverson et al., 2000; Kikutani et al., 2016; Meldrum and Roughton, 1933; Mitsuhashi et al., 2000; Xu et al., 2008). The α -CAs are found in humans, fungi, bacteria, and plants. α -CAs are the only class present in humans, and 15 CA isoforms have now been identified (Frost, 2014). These play essential roles in pH homeostasis, ion transport, bone resorption, calcification, and the biosynthetic reactions of fatty acids, amino acids and DNA, which makes them promising therapeutic targets against epilepsy, glaucoma, obesity, and cancer (Becker, 1955; De

Simone and Supuran, 2007; Mahon et al., 2015; Neri and Supuran, 2011; Supuran, 2008; Supuran, 2012). Most α -CAs are monomers or dimers, in which a catalytic zinc ion is coordinated by three histidine residues and a water molecule (Di Fiore et al., 2013; Eriksson et al., 1988). β -CAs are present in bacteria, yeast, algae, and plants (Neish, 1939; Smith et al., 1999). Since they are absent from humans and their activity is critical for the survival and virulence of pathogenic organisms, they have been considered potential targets of antimicrobial agents (Supuran, 2011). The fundamental structural units of β -CAs are dimers, but some also exist as tetramers, hexamers, and octamers (Kimber and Pai, 2000). β -CAs have two active site conformations (Rowlett, 2010). In the Type-I (open or R-state) configuration, a catalytic zinc ion is coordinated by two cysteines, one histidine and a water molecule. In the Type-II (closed or T-state) form, an aspartic acid residue replaces the zinc-coordinated water molecule, suggesting that it is an inactive form of the enzyme. Studies of Rv3588c of *Mycobacterium tuberculosis* have shown that switching between these two states is pH-dependent; it is active at pH 8.4 but not at pH 7.5 (Covarrubias et al., 2006; Suarez Covarrubias et al., 2005). The β -CAs are the only CA

* Corresponding author.

E-mail address: misunjin@gist.ac.kr (M.S. Jin).

<https://doi.org/10.1016/j.jsb.2019.07.011>

Received 15 June 2019; Received in revised form 29 July 2019; Accepted 30 July 2019

Available online 31 July 2019

1047-8477/ © 2019 The Author(s). Published by Elsevier Inc. This is an open access article under the CC BY-NC-ND license

(<http://creativecommons.org/licenses/by-nc-nd/4.0/>).

family to exhibit allosteric regulation. Prominent examples are the enzymes from *Haemophilus influenzae*, *Escherichia coli* and *Vibrio cholerae* in which a bicarbonate molecule also acts as a non-catalytic (inhibitory) site, its binding being accompanied by a substantial decrease of catalytic activity (Cronk et al., 2006; Ferraroni et al., 2015). Mycobacterial Rv1284 is also susceptible to redox-dependent inhibition in oxidizing conditions (Nienaber et al., 2015).

The β -CAs plays essential roles in the growth, development, virulence, and survival of fungi (Bahn et al., 2005; Cummins et al., 2014; Elleuche and Pöggeler, 2010; Hall et al., 2010; Klengel et al., 2005). The discovery that soluble adenylyl cyclase is directly regulated by bicarbonate provided a link between $\text{CO}_2/\text{HCO}_3^-$ sensing and cAMP signaling, which is very well conserved in fungi and is important for fungal pathogenicity (Chen et al., 2000; Hall et al., 2010; Klengel et al., 2005; Mogensen et al., 2006). Hemiascomycetous and basidiomycetous yeasts possess one or two β -CAs, while filamentous ascomycetes possess multiple β -CAs that differ in both cellular location and catalytic efficiency (Cleves et al., 1996). For example, *Cryptococcus neoformans* and *Cryptococcus gatti* have two β -CA genes, *can1* and *can2*, but only deletion of *can2* leads to a growth defect under ambient CO_2 conditions (Ren et al., 2014). In *Sordaria macrospora*, four CA genes (*cas1-4*), have been identified and their physiological roles characterized (Elleuche and Pöggeler, 2009); analysis of single gene deletion mutants showed that only deletion of *cas2* had a clear phenotypic effect, slowing both vegetative growth and ascospore germination, indicating that Cas2 is the major β -CA.

Four β -CA genes, *cafA-D*, have been found in *Aspergillus fumigatus* (Han et al., 2010). CafA and CafB are closely related proteins that belong to the plant-type β -CAs, whereas CafC and CafD are classified as cab-type. CafA and CafD are specifically translocated into mitochondria, while CafB and CafC are cytoplasmic. *cafA* and *cafB* are constitutively and strongly expressed, whereas *cafC* and *cafD* are weakly expressed but induced by high CO_2 concentration. This is an intriguing feature, since the major CAs exhibit low expression under high levels of CO_2 (Aguilera et al., 2005; Götz et al., 1999). The analysis of single and double deletion mutants has shown that CafA and CafB are the two major β -CAs in *A. fumigatus*, playing important roles in growth and conidiation, whereas CafC and CafD have only minor roles.

In this study we describe the crystal structures of CafC and CafD, and their biochemical characteristics. Both enzymes exhibited very low catalytic activities under our experimental conditions. On the basis of our results, we suggest the molecular mechanisms underlying their low catalytic activities; in CafC, the narrow opening blocks access of CO_2 to the active site while in CafD a unique arginine-to-glycine substitution results in loss of binding between a pair of aspartic acid and arginine residues (D-R pair), thereby, preventing a shift of the aspartic acid from acting as an on/off switch for enzyme activity. The CafD structure also reveals a novel binding site for “non-catalytic” zinc ion in the dimer interface, which may contribute to stabilizing the dimeric assembly.

2. Materials and methods

2.1. Cloning, protein expression and purification

Sequences encoding full-length CafC (residues 1–165, Genebank accession code EF486494.1) and CafD (residues 1–181, Genebank accession code AAHF01000013.1) of *Aspergillus fumigatus* were synthesized with codon-optimization (Gene Universal). They were cloned into pET21a and pET28b vectors, respectively, which express proteins with an N-terminal 6XHis tag and a thrombin protease cleavage site. Site-directed mutagenesis used overlap extension by PCR, and the enzymatic activities of the various mutants were determined. Verified constructs were transformed into *E. coli* BL21(DE3) cells for protein expression. Cells were grown in Lysogeny Broth (LB) medium at 37 °C. When the OD_{600} reached 0.6–0.8, protein expression was induced by incubation with 1 mM isopropyl- β -D-thiogalactopyranoside (IPTG) for 16 h at

20 °C. The cells were harvested by centrifugation at 14,000g for 15 min at 4 °C, and the cell pellet was resuspended in lysis buffer containing 20 mM Tris-HCl pH 8.0, 200 mM NaCl, 1 mM phenylmethylsulfonyl fluoride (PMSF), and 10 $\mu\text{g}/\text{mL}$ DNase I, and broken with a French Press. Insoluble debris was removed by centrifugation at 31,000g for 50 min at 4 °C. The supernatant was loaded onto a Ni-NTA agarose bead column (Incospharm) equilibrated with lysis buffer and eluted with a stepwise imidazole gradient from 50 to 500 mM. After thrombin cleavage to remove the 6XHis tag, the protein was further purified by HiTrap Q anion exchange chromatography (GE Healthcare) and Superdex 200 gel filtration chromatography (GE Healthcare) in a buffer containing 20 mM Tris-HCl pH 8.0 and 200 mM NaCl.

2.2. Glutaraldehyde cross-linking analysis

For chemical cross-linking with glutaraldehyde, purified protein (50 μM) in a buffer containing 20 mM HEPES pH 7.5 and 200 mM NaCl was mixed with various final concentrations of glutaraldehyde (Sigma-Aldrich). The mixtures were incubated for 1 h at room temperature, quenched with 20 mM Tris-HCl pH 8.0, and analyzed on 15% SDS-PAGE gels.

2.3. CO_2 hydration activity

In vitro CO_2 hydration was measured by the electrometric method (Carter et al., 1969). Briefly, CO_2 -saturated water was freshly prepared by bubbling CO_2 for at least 30 min. 4 mL of CO_2 -saturated water was rapidly mixed with 6 mL of purified protein (1 μM) in reaction buffer (20 mM Tris-HCl pH 8.5). CO_2 hydration activity was measured by determining the time required for the pH to drop from 8.3 to 6.3, and calculated in Wilbur-Anderson Units (WAU) according to the following definition: $\text{WAU} = (T_0 - T)/T$, where T_0 and T refer to the times in seconds taken in the absence and presence of enzyme, respectively (Wilbur and Anderson, 1948). CafA and CafB were used as positive controls. All assays were done in triplicate using the same enzyme preparation.

2.4. CaCO_3 precipitation activity

CaCO_3 precipitation activity was measured as previously described with slight modifications (Dreybrodt et al., 1997). Briefly, freshly prepared CO_2 -saturated water was mixed with the same volume of reaction buffer (1 M Tris-HCl pH 11.0 and 20 mM CaCl_2) with and without purified enzyme. The reaction cuvette was then sealed to prevent CO_2 leakage. Changes in absorbance at the wavelength of 600 nm were measured at 10 s intervals at 25 °C using a UV-vis spectrometer (Eppendorf). All measurements were performed three times using the same enzyme preparation.

3. Crystallization, data collection and structure determination

Purified enzyme was concentrated to 15–20 mg/mL for crystallization. CafC crystals were obtained by the sitting-drop vapor diffusion method by mixing 0.5 μL of protein and 0.5 μL of reservoir solution containing 1–3% (w/v) PEG2000 (or PEG5000MME) and 100 mM sodium acetate pH 4.5–5.5 at 22 °C. Crystals of CafD were grown in 24–28% (w/v) PEG3350, 200 mM MgCl_2 and 100 mM HEPES pH 7.0–7.5 (or Tris-HCl pH 9.0–9.5) at 22 °C. All crystals appeared within a day and continued to grow to full size in a week. Crystals of CafC and CafD were flash-frozen in liquid nitrogen with 22% and 5% glycerol as cryoprotectant, respectively. Diffraction data were collected at beamlines 7A and 11C of the Pohang Accelerator Laboratory (PAL), and were processed with the HKL2000 program package (Otwinowski and Minor, 1997). CafC and CafD structures were solved by molecular replacement with PHASER (McCoy et al., 2007) using the β -CA structures from *M. thermoautotrophicum* (Cab, PDB code 1G5C) (Strop et al., 2001) and A.

fumigatus (CafA, PDB code 6JOT), respectively. Models were built by several rounds of modification in COOT (Emsley and Cowtan, 2004) and subjected to refinement using REFMAC5 (Murshudov et al., 1997) and PHENIX (Adams et al., 2010). Residues 1–8 of the N-terminus of CafD were not visible in the electron density map, and were not included in the final model. Using MOLPROBITY (Davis et al., 2007), all residues were confirmed to lie in the allowed region of the Ramachandran plot. The X-ray crystallographic data and refinement statistics are summarized in Supplementary Table 1. All figures in the manuscript were produced using PyMOL (www.pymol.org).

4. Results and discussion

4.1. The low catalytic activity CafC and CafD

In order to examine the catalytic activities of CafC and CafD, the genes were cloned, overexpressed and purified. The homodimeric states of CafC and CafD in solution were confirmed by gel filtration profiles and chemical cross-linking with glutaraldehyde (Supplementary Fig. 1). We observed that unlike the major β -CAs of *A. fumigatus*, CafA and CafB, which have substantial apparent CO_2 hydrolysis activity *in vitro*, the minor β -CAs, CafC and CafD, exhibited very low activities, as seen by the much slower declines of pH accompanying proton release during CO_2 hydration (Fig. 1). Both enzymes exhibited specific activities of approximately 2.4 WAU/mg, 8- and 10-fold lower than those of CafA (20 WAU/mg) and CafB (25 WAU/mg), respectively. These low activities of CafC and CafD were consistent with the finding of Han et al. (2010) that the levels of *cafC* and *cafD* mRNAs were approximately 10–100 times lower than those of *cafA* and *cafB* at both ambient and elevated CO_2 concentrations (Han et al., 2010). CafC is known to play only a minor role in conidiation, and there is little CafD activity in almost all the developmental stages of *A. fumigatus*.

4.2. Overall structures of CafC and CafD

To understand the molecular mechanisms underlying the low catalytic activities of CafC and CafD, the purified proteins were crystallized and their structures were determined at 1.8 and 1.9 Å resolution, respectively. The final model of CafC contained all 165 amino acids, whereas the first eight N-terminal amino acids of CafD were absent from the final CafD structure (Supplementary Fig. 2). The N-terminal sequence of CafD has been predicted to contain the mitochondrial targeting sequence, and analysis using the MitoFates program revealed a potential cleavage site at position 10 (Fukasawa et al., 2015; Han

et al., 2010). In agreement with the observations of oligomeric states in solution (Supplementary Fig. 1), the crystal structures CafC and CafD consisted of cab-type dimers formed by equivalent monomers, with the catalytic zinc-binding site located at the interface between the monomers (Fig. 2). Both crystal forms contain a dimer within the asymmetric unit.

As in other β -CAs (Nienaber et al., 2015; Strop et al., 2001; Suarez Covarrubias et al., 2005), the CafC monomer consists of an N-terminal α -helical extension, a conserved central α/β fold, and a C-terminal subdomain (Fig. 2A and 2B). The N-terminal α -helix extends away from the body of the molecule and creates extensive interfacial contacts that bind together the sister monomers. The α/β core consists mainly of a parallel four-stranded β -sheet (β_2 - β_1 - β_3 - β_4) flanked by a fifth antiparallel β -strand (β_5). The β -sheets in each monomer pack together in antiparallel manner, forming a continuous 10-stranded β -sheet structure across the two monomers. As in some mycobacterial β -CAs, the C-terminal subdomain of CafC protrudes towards the adjacent monomer making additional intermolecular contacts and further stabilizing the dimeric structure (Fig. 2B and Supplementary Fig. 3) (Strop et al., 2001; Suarez Covarrubias et al., 2005).

CafD is architecturally quite different from CafC in three respects. The first is the lack of an N-terminal α -helical arm (Fig. 2C and 2D). The second is that the CafD monomer contains a sixth antiparallel β -strand that associates with the parallel five-stranded β -sheet (β_3 - β_2 - β_4 - β_5 - β_6 - β_1) to form an extended 12-stranded β -sheet across the dimer. To the best of our knowledge, this β -sheet fold is unique to CafD. The third difference is that, as in other fungal β -CAs, the C-terminal subdomain lies above the core region within the same monomer, forming the molecular surface (Fig. 2D and Supplementary Fig. 4) (Lehneck et al., 2014; Russell et al., 2008; Schlicker et al., 2009). In the rest of an article, prime notations are used for the residues of one monomer to differentiate them from those of the other monomer.

4.3. Two leucines partially block access to the active site of CafC

CafC has a Type-I or open conformation in which the catalytic zinc ion is tetrahedrally coordinated by three conserved residues (C36, H88, C91) and a water molecule (Fig. 3A). The water molecule is strongly anchored by hydrogen bonding with the strictly conserved D38, which is oriented in this position by salt bridges with R40. This highly conserved D-R pair has been found in all CA structures with open conformations, and is thought to mediate proton shuffling and/or $\text{CO}_2/\text{HCO}_3^-$ interconversion (Provart et al., 1993; Rowlett et al., 2009; Smith et al., 2002). Structural comparisons demonstrate that the low activity of CafC may be due to the fact that its active site is smaller than those of other cab-type β -CAs, and is almost completely shielded from solvent by the significant inward movement of a loop connecting the N-terminal helical arm to β -strand 1 in the neighboring monomer (Fig. 3B and Supplementary Fig. 5) (Lehneck et al., 2014; Schlicker et al., 2009; Strop et al., 2001; Teng et al., 2009). In particular, L25' on this loop, which protrudes into the active site, may play a key role as gatekeeper hindering substrate diffusion, substrate positioning at the active site, and/or product release. In addition, L78' is located right behind L25', and has a role in stabilizing the conformation of L25' through van der Waals interactions, and so may contribute to lowering catalytic activity (Fig. 3B).

To confirm the proposed roles of these two leucine residues, we performed site-directed mutagenesis. A CafC variant harboring an L25G single mutation gave a substantial increase in response to CO_2 compared to the wild-type, while a CafC double mutant at positions 25 and 78 showed a > 16-fold increase in catalytic activity (Fig. 3C). The enhanced catalytic activity of the double mutant was further confirmed by CaCO_3 precipitation assays (Fig. 3D). The L78G single mutant displayed a small but clear-cut increase in both CO_2 hydration and CaCO_3 precipitation activity (Fig. 3C and D). This may be because loss of L78 increases the local structural flexibility of L25. The fact that the

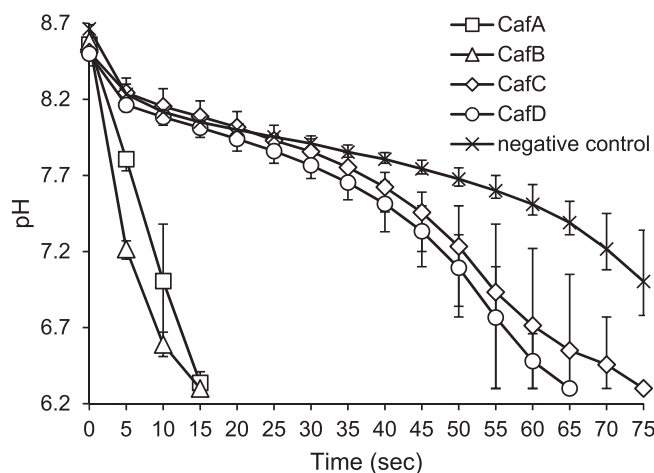


Fig. 1. Low enzymatic activities of CafC and CafD. Time courses of CO_2 hydration by 1 μM of purified proteins. Data are means (\pm standard deviations, SDs) of three independent experiments using the same preparation. Error bars represent SDs.

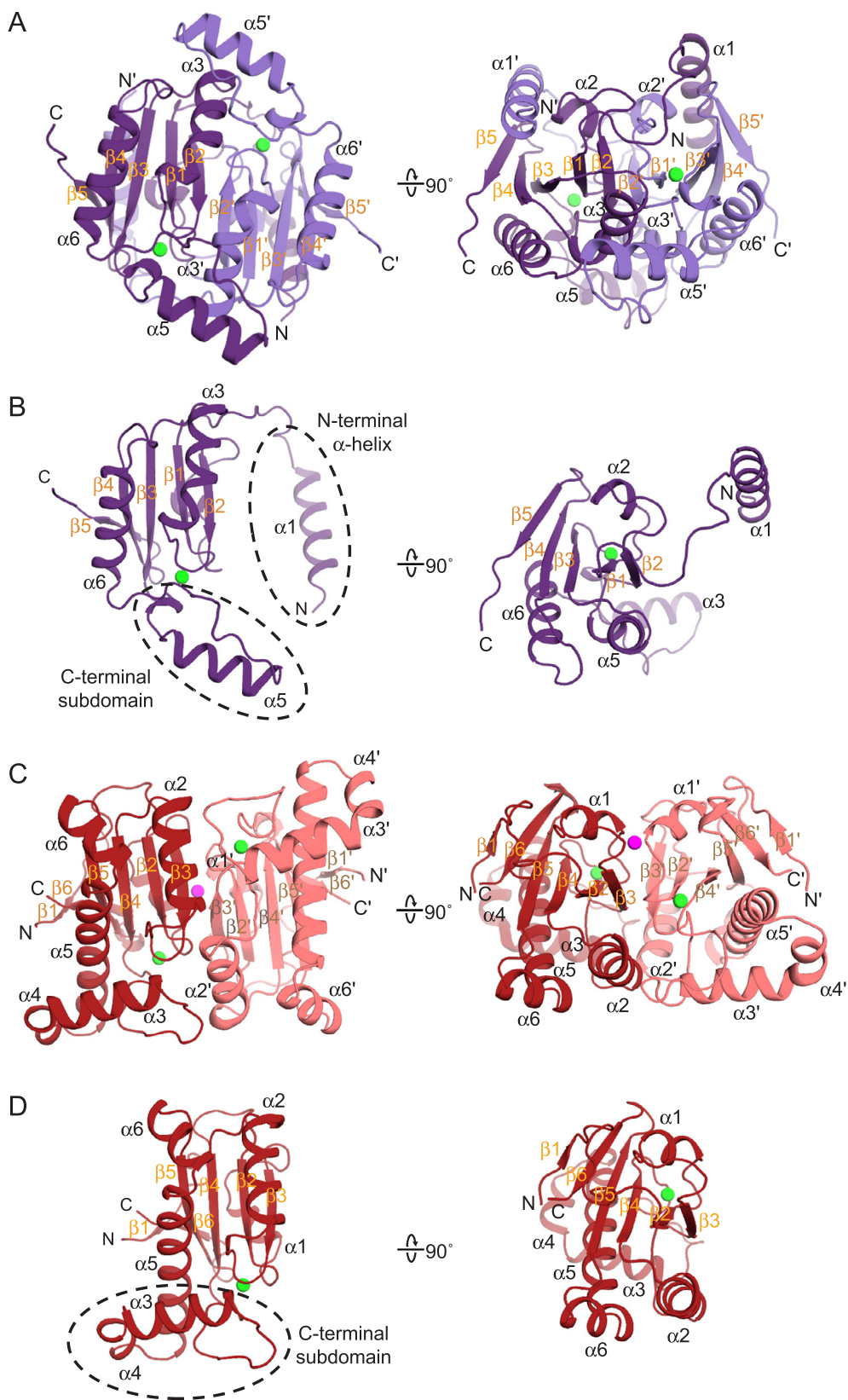


Fig. 2. Overall structures of CafC and CafD. (A) Dimeric and (B) monomeric fold of CafC. (C) Dimeric and (D) monomeric fold of CafD. The individual monomers are shown in purple and light purple, and red and pink, respectively. The catalytic and non-catalytic zinc ions are shown as green and magenta spheres, respectively. The subdomains within each monomer are marked by black dashed circles.

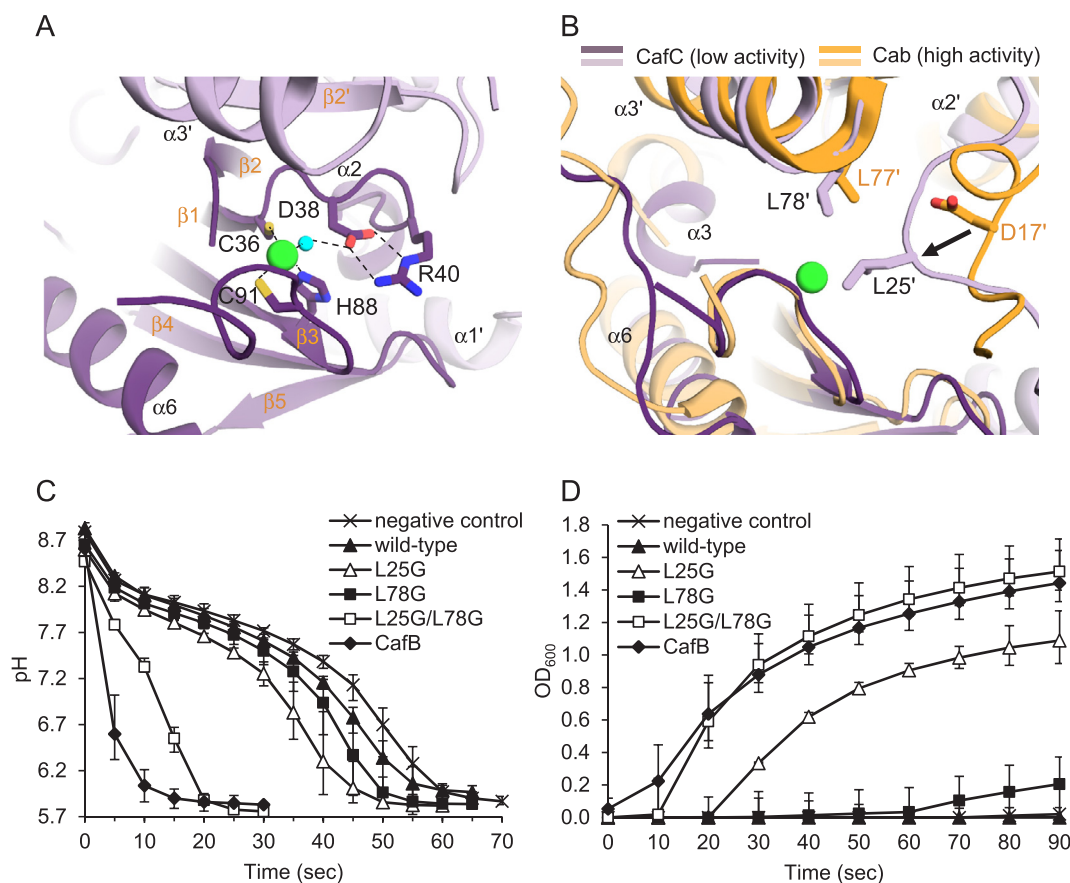


Fig. 3. The CafC active site. (A) Close-up view of zinc coordination. Residues involved in zinc coordination and formation of the D-R pair are shown in stick representation. The zinc ion and water molecule are shown as green and cyan spheres, respectively, and interactions are indicated by dashed lines. (B) Comparison of the active sites of CafC (low activity) and Cab (high activity) from *M. thermoautotrophicum*. Residues around the catalytic entry site are shown in stick representation. A significant structural difference is marked by the black arrow. (C) CO₂ hydration and (D) CaCO₃ precipitation by CafC mutants (L25G and/or L78G) by 2 μM and 1.4 μM protein suspensions, respectively. Each point is the mean of three different replicate experiments, each performed in triplicate. Error bars indicate SDs.

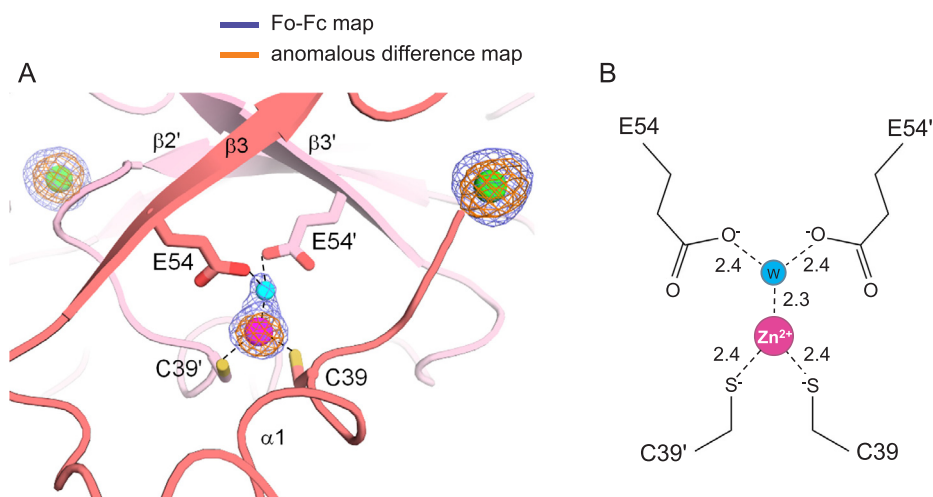


Fig. 4. Binding of the non-catalytic zinc at the CafD dimer interface. (A) Residues involved in the non-catalytic zinc coordination are shown in stick representation. The blue mesh represents the Fo-Fc map contoured at 5σ. An anomalous difference map (contoured at 3σ) for non-catalytic zinc ion is shown in orange mesh. Helix 1 (α1) is shown as loop for clarity. Catalytic zinc, non-catalytic zinc and water molecules are shown as green, magenta, and cyan spheres, respectively. (B) Schematic representation of the zinc-chelating ligands at the CafD dimer interface. The non-catalytic zinc (Zn²⁺) ion and water molecule (W) are shown as magenta and cyan spheres, respectively. All distances are in angstroms.

structures of the wild-type and the double mutant were practically identical, with C α rmsd values < 0.3 Å, suggests that the increased catalytic activities of the double mutant were not due to substantial changes of overall structure (Supplementary Fig. 6). Collectively, our results suggest that simultaneous substitution of L25 and L78 is critical for providing adequate access of substrate to the active site of the enzyme.

5. Binding of non-catalytic zinc at the dimer interface of CafD

In the CafD structure, a strong and positive signal in the Fo-Fc map (> 5σ), distinct from the electron density of the water molecule, was observed at the solvent-accessible dimer interface, suggesting the presence of a metal ion (Fig. 2C and 4A). It had a temperature factor of 55.3 Å² and an occupancy of 1.0. We observed that this metal ion, which is derived from natural sources during cell culture, is coordinated in a 3-coordinate geometry involving juxtaposed cysteine residues

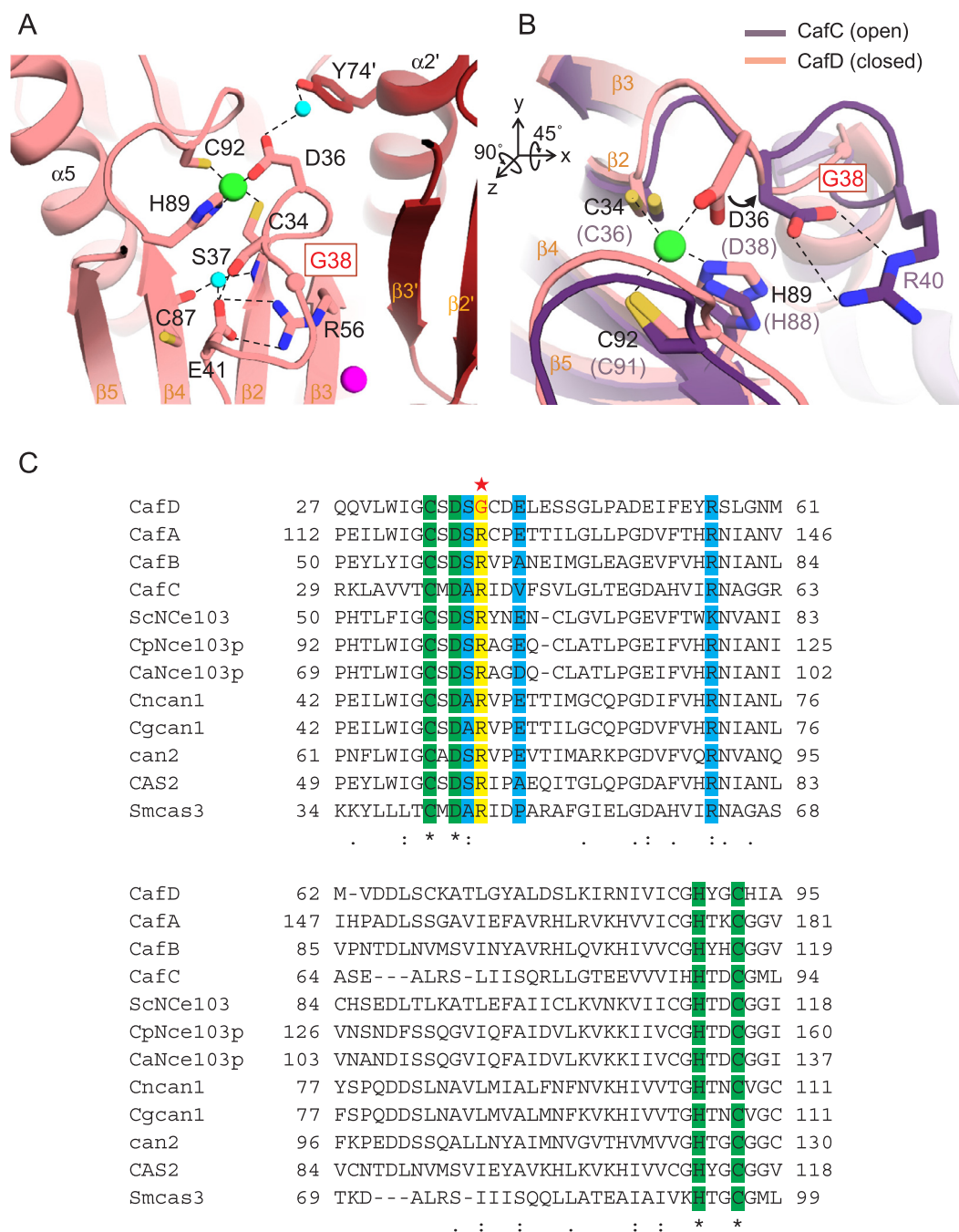


Fig. 5. The CafD active site. (A) Residues involved in zinc coordination and the salt bridge network in the active site are depicted in stick representation. G38 residue in CafD is labeled in red and shown as a pink ball. Catalytic zinc, non-catalytic zinc and water molecules are shown as green, magenta, and cyan spheres, respectively. (B) Comparison of the active sites of CafC (open form) and CafD (closed form). The aspartic acid shift is indicated by a black arrow. Some residues of CafC that are superimposable with those of CafD are written in parentheses. (C) Sequence alignment of the active site residues of CafD and fungal β -CAs from *A. fumigatus* (CafA-C), *S. cerevisiae* (ScNce103), *C. parapsilosis* (CpNce103p), *C. albicans* (CaNce103p), *S. macrospora* (CAS2, CAS3), *C. gatti* (Can1), and *C. neoformans* (Can1, Can2). Residues involved in zinc coordination (closed configuration) and the conserved arginine residue in the D-R pair are highlighted in green and yellow, respectively. The arginine-to-glycine substitution only found in CafD is written in red and highlighted by the star. Residues involved in the salt bridge network of CafD (shown in Fig. 5A) and their equivalents in other β -CAs are highlighted in cyan.

(C39) at the dimer interface, forming a bond angle of approximately 120° with the water molecule (Fig. 4B). The pair of symmetry-related glutamic acids (E54) are not directly involved in the coordination of a metal ion, but serve to hold and correctly orient the water molecule in the third coordination site. Since only Fe^{2+} , Co^{2+} , Ni^{2+} , Cu^{2+} or Zn^{2+} can be coordinated by the sulfur in cysteine, we analyzed X-ray fluorescence (XRF) spectra and the combined phases obtained by molecular replacement and single-wavelength anomalous diffraction (SAD) to

identify the bound element and establish its location in CafD. An XRF scan at the K-edge region of the corresponding metal showed that the sample was only excited near the zinc absorption K-edge (9,671 eV or $\lambda = 1.2820 \text{ \AA}$) (Supplementary Fig. 7). This suggested that the CafD crystal contains only one type of metal, namely zinc (II) ion. An anomalous difference map calculated from data collected at the zinc edge showed peaks of 3σ at the predicted three binding sites, two in the catalytic core and one at the dimer interface, indicating that the metal

assignment was correct (Fig. 4). To the best of our knowledge, this is the first crystal structure of a CA in complex with a “non-catalytic” zinc ion in the dimer interface. As mentioned above, the CafD structure lacks the N-terminal α -helical extension, which makes extensive contacts with the neighboring monomer (Fig. 2C and 2D). The binding of non-catalytic zinc ion at the dimer interface is likely to compensate to some extent for the absence of the interfacial interactions involving this N-terminal arm, and thus to contribute to dimer stability. To confirm the proposed role of non-catalytic zinc in CafD stabilization, we generated the variant with double mutation (C39A and E54A) in the non-catalytic zinc coordinating sphere. However, it was barely expressed as a soluble protein in *E. coli* system (data not shown). The double mutant may no longer directly coordinate the non-catalytic zinc ion at the CafD dimer interface, leading to have a high tendency to misfold and/or lose the native structure. Together, our data suggest that this apparently unique non-catalytic zinc in CafD has a potential effect on stable formation of the dimeric assembly, and its deficiency can lead to loss or improper physiological function of CafD.

5.1. Absence of the conserved D-R pair from the CafD active site

Comparison of the CafC and CafD structures shows that unlike the zinc-binding site of CafC, which is largely shielded from solvent by the loop containing L25', that of CafD is very exposed to solution due to the absence of the corresponding loop (Fig. 3B and Supplementary Fig. 8). This suggests that a different mechanism underlies the low catalytic activity of CafD. The CafD structure reveals that all its zinc coordination sites are occupied by amino acids as ligands involving C34, H89, C92, and D36, which replace the zinc-bound water, thus yielding a Type-II or closed conformation (Fig. 5A). The conformation of D36 is strongly anchored by a water-mediated hydrogen bond with Y74' from the sister monomer. Unexpectedly, we observed that an arginine that is strictly conserved within the β -CA family is substituted by glycine at position 38, so that D36 cannot form a D-R pair that orients D36 in an ideal way for accepting a zinc-bound water molecule (Fig. 5B). Structure-based sequence alignment shows that this arginine-to-glycine substitution only occurs in CafD (Fig. 5C and Supplementary Fig. 9). The flexibility of glycine also permits flipping of peptide bonds, leading to dramatic local rearrangements. As a result, a network of salt bridge interactions involving residues S37, E41, and R56 is formed, locking CafD in a catalytically inactive state by preventing the conformational change of D36 through steric hindrance by F53' (Fig. 5A and Supplementary Fig. 10). Water-mediated hydrogen bonds between E41, the backbone nitrogen of C34 and the backbone oxygen of C87 further stabilize the inactive state by orienting E41 for effective interaction with S37 and R56 (Fig. 5A). These three conserved residues are also found in some other β -CAs, but they do not form the same atomic interactions (Fig. 5C and Supplementary Fig. 11). The pKa values of these amino acids indicate that the salt bridges would be sustained between pH 6 and pH10. Because the mitochondrial matrix has a pH of approximately 7.8, CafD may exist predominantly in this inactive form in under physiological conditions, which explains why it has very low catalytic activity *in vivo* and *in vitro* (Fig. 1) (Han et al., 2010). Further research is required to define the specific role of CafD in mitochondria.

In summary, we have determined the first structures of the minor fungal β -CAs, CafC and CafD, of *A. fumigatus*, and provided insight into the reasons for their low enzymatic activities. Structure-based mutagenesis data together with their crystal structures point to distinct mechanisms governing their low catalytic activities. CafC shows low activity due to poor substrate access to the active site, while CafD is predominantly inactive because a characteristic shift of an aspartic acid, which results from formation of a D-R pair and can switch the enzyme to the active form, is inhibited by substitution of a glycine for the arginine. Furthermore, this unique substitution of glycine may provide the structural flexibility necessary for the formation of local network of salt bridges that further stabilizes CafD in an inactive state.

We have also identified a novel binding site for non-catalytic zinc ion in the CafD dimer interface. The incorporation of non-catalytic zinc as a cofactor may compensate for the loss of the N-terminal α -helical extension, and thus contribute to stabilizing the dimeric assembly.

Acknowledgements

We thank the staff at beamlines 7A and 11C of the Pohang Accelerator Laboratory (PAL). We are grateful to Dr. Julian Gross for critical reading of the manuscript. This work was supported by grants from the National Research Foundation (NRF), funded by the Ministry of Science, ICT, and Future Planning of Korea (grant numbers: NRF-2017R1A2B4003278 and NRF-2017M3A9F6029753).

Accession codes

Coordinates and structure factors for CafC have been deposited in the Protein Data Bank under accession codes 6JQC (the wild-type) and 6JQD (L23G/L78G mutant). Coordinates and structure factors for the wild-type CafD have been deposited under accession code 6JQE.

Declaration of Competing Interests

The authors declare no competing financial interests.

Author contributions

All authors contributed to this work by designing the study, conducting experiments, discussing the results and commenting on the manuscript. S.K., N.J.K., and S.K. expressed and purified the enzymes, crystallized them and determined their crystal structures. N.J.K. and S.H. assayed the activities of the enzymes. J.S. made the plasmid constructs and performed high-throughput crystallization screening. S.K. and N.J.K. prepared the figures and S.K. and M.S.J. wrote the manuscript. All authors read and approved the manuscript for submission.

Appendix A. Supplementary data

Supplementary data to this article can be found online at <https://doi.org/10.1016/j.jsb.2019.07.011>.

References

- Adams, P.D., Afonine, P.V., Bunkóczi, G., Chen, V.B., Davis, I.W., Echols, N., Headd, J.J., Hung, L.W., Kapral, G.J., Grosse-Kunstleve, R.W., McCoy, A.J., Moriarty, N.W., Oeffner, R., Read, R.J., Richardson, D.C., Richardson, J.S., Terwilliger, T.C., Zwart, P.H., 2010. PHENIX: a comprehensive Python-based system for macromolecular structure solution. *Acta Crystallogr. Sec. D-Biol. Crystallogr.* 66, 213–221.
- Aguilera, J., Petit, T., de Winde, J.H., Pronk, J.T., 2005. Physiological and genome-wide transcriptional responses of *Saccharomyces cerevisiae* to high carbon dioxide concentrations. *FEMS Yeast Res.* 5, 579–593.
- Bahn, Y.S., Cox, G.M., Perfect, J.R., Heitman, J., 2005. Carbonic anhydrase and CO₂ sensing during *Cryptococcus neoformans* growth, differentiation, and virulence. *Curr. Biol.* 15, 2013–2020.
- Becker, B., 1955. The mechanism of the fall in intraocular pressure induced by the carbonic anhydrase inhibitor, diamox. *Am. J. Ophthalmol.* 39, 177–184.
- Carter, J.M., Havard, D.J., Parsons, D.S., 1969. Electrometric assay of rate of hydration of CO₂ for investigation of kinetics of carbonic anhydrase. *J. Physiol.* 204, 60P–62P.
- Chen, Y., Cann, M.J., Litvin, T.N., Iourgenko, V., Sinclair, M.L., Levin, L.R., Buck, J., 2000. Soluble adenylyl cyclase as an evolutionarily conserved bicarbonate sensor. *Science* 289, 625–628.
- Cleves, A.E., Cooper, D.N.W., Barondes, S.H., Kelly, R.B., 1996. A new pathway for protein export in *Saccharomyces cerevisiae*. *J. Cell Biol.* 133, 1017–1026.
- Covarrubias, A.S., Bergfors, T., Jones, T.A., Högbom, M., 2006. Structural mechanics of the pH-dependent activity of beta-carbonic anhydrase from *Mycobacterium tuberculosis*. *J. Biol. Chem.* 281, 4993–4999.
- Cronk, J.D., Rowlett, R.S., Zhang, K.Y., Tu, C., Endrizzi, J.A., Lee, J., Gareiss, P.C., Preiss, J.R., 2006. Identification of a novel noncatalytic bicarbonate binding site in eubacterial β -carbonic anhydrase. *Biochemistry* 45, 4351–4361.
- Cummins, E.P., Selfridge, A.C., Sporn, P.H., Sznajder, J.I., Taylor, C.T., 2014. Carbon dioxide-sensing in organisms and its implications for human disease. *Cell. Mol. Life Sci.* 71, 831–845.

- Davis, I.W., Leaver-Fay, A., Chen, V.B., Block, J.N., Kapral, G.J., Wang, X., Murray, L.W., Arendall, W.B., Snoeyink, J., Richardson, J.S., Richardson, D.C., 2007. MolProbity: all-atom contacts and structure validation for proteins and nucleic acids. *Nucleic Acids Res.* 35, W375–W383.
- De Simone, G., Supuran, C.T., 2007. Antiobesity carbonic anhydrase inhibitors. *Curr. Top. Med. Chem.* 7, 879–884.
- Del Prete, S., Vullo, D., Scozzafava, A., Capasso, C., Supuran, C.T., 2014a. Cloning, characterization and anion inhibition study of the δ -class carbonic anhydrase (TweCA) from the marine diatom *Thalassiosira weissflogii*. *Bioorg. Med. Chem.* 22, 531–537.
- Del Prete, S., Vullo, D., Fisher, G.M., Andrews, K.T., Poulsen, S.A., Capasso, C., Supuran, C.T., 2014b. Discovery of a new family of carbonic anhydrases in the malaria pathogen *Plasmodium falciparum*—The η -carbonic anhydrases. *Bioorg. Med. Chem. Lett.* 24, 4389–4396.
- Di Fiore, A., Capasso, C., De Luca, V., Monti, S.M., Carginale, V., Supuran, C.T., Scozzafava, A., Pedone, C., Rossi, M., De Simone, G., 2013. X-ray structure of the first 'extremo- α -carbonic anhydrase', a dimeric enzyme from the thermophilic bacterium *Sulfolobus solfataricus*. *Acta Crystallogr. Sect. D-Biol. Crystallogr.* 69, 1150–1159.
- Dreybrodt, W., Eisenlohr, L., Madry, B., Ringer, S., 1997. Precipitation kinetics of calcite in the system $\text{CaCO}_3\text{-H}_2\text{O-CO}_2$: The conversion to CO_2 by the slow process $\text{H}^+ + \text{HCO}_3^- > \text{CO}_2 + \text{H}_2\text{O}$ as a rate limiting step. *Geochim. Cosmochim. Acta* 61, 3897–3904.
- Elleuche, S., Pöggeler, S., 2009. Evolution of carbonic anhydrases in fungi. *Curr. Genet.* 55, 211–222.
- Elleuche, S., Pöggeler, S., 2010. Carbonic anhydrases in fungi. *Microbiol.-Sgm* 156, 23–29.
- Emsley, P., Cowtan, K., 2004. Coot: model-building tools for molecular graphics. *Acta Crystallogr. D Biol. Crystallogr.* 60, 2126–2132.
- Eriksson, A.E., Jones, T.A., Liljas, A., 1988. Refined structure of human carbonic anhydrase II at 2.0 Å resolution. *Proteins* 4, 274–282.
- Ferraroni, M., Del Prete, S., Vullo, D., Capasso, C., Supuran, C.T., 2015. Crystal structure and kinetic studies of a tetrameric type II β -carbonic anhydrase from the pathogenic bacterium *Vibrio cholerae*. *Acta Crystallogr. D Biol. Crystallogr.* 71, 2449–2456.
- Frost, S.C., 2014. Physiological functions of the α class of carbonic anhydrases. *Subcell. Biochem.* 75, 9–30.
- Fukasawa, Y., Tsuji, J., Fu, S.C., Tomii, K., Horton, P., Imai, K., 2015. MitoFates: improved prediction of mitochondrial targeting sequences and their cleavage sites. *Mol. Cell. Proteomics* 14, 1113–1126.
- Götz, R., Gnann, A., Zimmermann, F.K., 1999. Deletion of the carbonic anhydrase-like gene *NCE103* of the yeast *Saccharomyces cerevisiae* causes an oxygen-sensitive growth defect. *Yeast* 15, 855–864.
- Hall, R.A., De Sordi, L., MacCallum, D.M., Topal, H., Eaton, R., Bloor, J.W., Robinson, G.K., Levin, L.R., Buck, J., Wang, Y., Gow, N.A.R., Steegborn, C., Mühlischlegel, F.A., 2010. CO_2 acts as a signalling molecule in populations of the fungal pathogen *Candida albicans*. *Plos Pathogens* 6.
- Han, K.H., Chun, Y.H., Figueiredo, B.D.P., Soriani, F.M., Savoldi, M., Almeida, A., Rodrigues, F., Cairns, C.T., Bignell, E., Tobal, J.M., Goldman, M.H.S., Kim, J.H., Bahn, Y.S., Goldman, G.H., Ferreira, M.E.D., 2010. The conserved and divergent roles of carbonic anhydrases in the filamentous fungi *Aspergillus fumigatus* and *Aspergillus nidulans*. *Mol. Microbiol.* 75, 1372–1388.
- Hasinoff, B.B., 1984. Kinetics of carbonic anhydrase catalysis in solvents of increased viscosity: a partially diffusion-controlled reaction. *Arch. Biochem. Biophys.* 233, 676–681.
- Iverson, T.M., Alber, B.E., Kisker, C., Ferry, J.G., Rees, D.C., 2000. A closer look at the active site of γ -class carbonic anhydrases: High-resolution crystallographic studies of the carbonic anhydrase from *Methanosarcina thermophila*. *Biochemistry* 39, 9222–9231.
- Kikutani, S., Nakajima, K., Nagasato, C., Tsuji, Y., Miyatake, A., Matsuda, Y., 2016. Thylakoid luminal θ -carbonic anhydrase critical for growth and photosynthesis in the marine diatom *Phaeodactylum tricorutum*. *PNAS* 113, 9828–9833.
- Kimber, M.S., Pai, E.F., 2000. The active site architecture of *Pisum sativum* β -carbonic anhydrase is a mirror image of that of α -carbonic anhydrases. *EMBO J.* 19, 1407–1418.
- Klengel, T., Liang, W.J., Chaloupka, J., Ruoff, C., Schröppel, K., Naglik, J.R., Eckert, S.E., Mogensen, E.G., Haynes, K., Tuite, M.F., Levin, L.R., Buck, J., Mühlischlegel, F.A., 2005. Fungal adenyl cyclase integrates CO_2 sensing with cAMP signaling and virulence. *Curr. Biol.* 15, 2021–2026.
- Lehneck, R., Neumann, P., Vullo, D., Elleuche, S., Supuran, C.T., Ficner, R., Pöggeler, S., 2014. Crystal structures of two tetrameric β -carbonic anhydrases from the filamentous ascomycete *Sordaria macrospora*. *FEBS J.* 281, 1759–1772.
- Badger, M.R., Price, G.D., 1994. The role of carbonic anhydrase in photosynthesis. *Ann. Rev. Plant Physiol. Plant Mol. Biol.* 45, 369–392.
- Mahon, B.P., Pinard, M.A., McKenna, R., 2015. Targeting carbonic anhydrase IX activity and expression. *Molecules* 20, 2323–2348.
- Mccooy, A.J., Grosse-Kunstleve, R.W., Adams, P.D., Winn, M.D., Storoni, L.C., Read, R.J., 2007. Phaser crystallographic software. *J. Appl. Crystallogr.* 40, 658–674.
- Meldrum, N.U., Roughton, F.J., 1933. Carbonic anhydrase. Its preparation and properties. *J. Physiol.* 80, 113–142.
- Mitsuhashi, S., Mizushima, T., Yamashita, E., Yamamoto, M., Kumasaka, T., Moriyama, H., Ueki, T., Miyachi, S., Tsukihara, T., 2000. X-ray structure of β -carbonic anhydrase from the red alga, *Porphyridium purpureum*, reveals a novel catalytic site for CO_2 hydration. *J. Biol. Chem.* 275, 5521–5526.
- Mogensen, E.G., Janbon, G., Chaloupka, J., Steegborn, C., Fu, M.S., Moyrand, F., Klengel, T., Pearson, D.S., Geeves, M.A., Buck, J., Levin, L.R., Mühlischlegel, F.A., 2006. *Cryptococcus neoformans* senses CO_2 through the carbonic anhydrase Can2 and the adenyl cyclase Cac1. *Eukaryot. Cell* 5, 103–111.
- Murshudov, G.N., Vagin, A.A., Dodson, E.J., 1997. Refinement of macromolecular structures by the maximum-likelihood method. *Acta Crystallogr. Sect. D-Struct. Biol.* 53, 240–255.
- Neish, A.C., 1939. Studies on chloroplasts: Separation of chloroplasts, a study of factors affecting their flocculation and the calculation of the chloroplast content of leaf tissue from chemical analysis. *Biochem. J.* 33, 293–299.
- Neri, D., Supuran, C.T., 2011. Interfering with pH regulation in tumours as a therapeutic strategy. *Nat. Rev. Drug. Discov.* 10, 767–777.
- Nienaber, L., Cave-Freeman, E., Cross, M., Mason, L., Bailey, U.M., Amani, P., Davis, R.A., Taylor, P., Hofmann, A., 2015. Chemical probing suggests redox-regulation of the carbonic anhydrase activity of mycobacterial Rv1284. *FEBS J.* 282, 2708–2721.
- Otwinski, Z., Minor, W., 1997. Processing of X-ray diffraction data collected in oscillation mode. *Macromol. Crystallogr.* 276 (Pt A), 307–326.
- Pocker, Y., Janjić, N., 1987. Enzyme kinetics in solvents of increased viscosity. Dynamic aspects of carbonic anhydrase catalysis. *Biochemistry* 26, 2597–2606.
- Provart, N.J., Majeau, N., Coleman, J.R., 1993. Characterization of pea chloroplastic carbonic anhydrase. Expression in *Escherichia coli* and site-directed mutagenesis. *Plant Mol. Biol.* 22, 937–943.
- Ren, P., Chaturvedi, V., Chaturvedi, S., 2014. Carbon dioxide is a powerful inducer of monokaryotic hyphae and spore development in *Cryptococcus gattii* and carbonic anhydrase activity is dispensable in this dimorphic transition. *PLoS One* 9.
- Rowlett, R.S., 2010. Structure and catalytic mechanism of the β -carbonic anhydrases. *Biochim. Biophys. Acta Proteins Proteomics* 1804, 362–373.
- Rowlett, R.S., Tu, C., Lee, J., Herman, A.G., Chapnick, D.A., Shah, S.H., Gareiss, P.C., 2009. Allosteric site variants of *Haemophilus influenzae* β -carbonic anhydrase. *Biochemistry* 48, 6146–6156.
- Russell, R.J., Kerry, P.S., Stevens, D.J., Steinhauer, D.A., Martin, S.R., Gamblin, S.J., Skehel, J.J., 2008. Structure of influenza hemagglutinin in complex with an inhibitor of membrane fusion. *Proc. Natl. Acad. Sci. USA* 105, 17736–17741.
- Schlicker, C., Hall, R.A., Vullo, D., Middelhaufe, S., Gertz, M., Supuran, C.T., Mühlischlegel, F.A., Steegborn, C., 2009. Structure and inhibition of the CO_2 -sensing carbonic anhydrase Can2 from the pathogenic fungus *Cryptococcus neoformans*. *J. Mol. Biol.* 385, 1207–1220.
- Smith, K.S., Ingram-Smith, C., Ferry, J.G., 2002. Roles of the conserved aspartate and arginine in the catalytic mechanism of an archaeal β -class carbonic anhydrase. *J. Bacteriol.* 184, 4240–4245.
- Smith, K.S., Jakubczik, C., Whittam, T.S., Ferry, J.G., 1999. Carbonic anhydrase is an ancient enzyme widespread in prokaryotes. *Proc. Natl. Acad. Sci. USA* 96, 15184–15189.
- Strop, P., Smith, K.S., Iverson, T.M., Ferry, J.G., Rees, D.C., 2001. Crystal structure of the "cab"-type β class carbonic anhydrase from the archaeon *Methanobacterium thermoautotrophicum*. *J. Biol. Chem.* 276, 10299–10305.
- Suarez Covarrubias, A., Larsson, A.M., Högbom, M., Lindberg, J., Bergfors, T., Björkelid, C., Mowbray, S.L., Unge, T., Jones, T.A., 2005. Structure and function of carbonic anhydrases from *Mycobacterium tuberculosis*. *J. Biol. Chem.* 280, 18782–18789.
- Supuran, C.T., 2008. Carbonic anhydrases: novel therapeutic applications for inhibitors and activators. *Nat. Rev. Drug Discov.* 7, 168–181.
- Supuran, C.T., 2011. Bacterial carbonic anhydrases as drug targets: toward novel anti-biotics? *Front. Pharmacol.* 2.
- Supuran, C.T., 2012. Structure-based drug discovery of carbonic anhydrase inhibitors. *J. Enzyme Inhib. Med. Chem.* 27, 759–772.
- Teng, Y.B., Jiang, Y.L., He, Y.X., He, W.W., Lian, F.M., Chen, Y., Zhou, C.Z., 2009. Structural insights into the substrate tunnel of *Saccharomyces cerevisiae* carbonic anhydrase Nce103. *BMC Struct. Biol.* 9, 67.
- Wilbur, K.M., Anderson, N.G., 1948. Electrometric and colorimetric determination of carbonic anhydrase. *J. Biol. Chem.* 176, 147–154.
- Xu, Y., Feng, L., Jeffrey, P.D., Shi, Y.G., Morel, F.M.M., 2008. Structure and metal exchange in the cadmium carbonic anhydrase of marine diatoms. *Nature* 452, 56–U53.